Singular Vectors and Time-Dependent Normal Modes of a Baroclinic Wave-Mean Oscillation

CHRISTOPHER L. WOLFE* AND ROGER M. SAMELSON

College of Oceanic and Atmospheric Sciences, Oregon State University, Corvallis, Oregon

ABSTRACT

Linear disturbance growth is studied in a quasigeostrophic baroclinic channel model with several thousand degrees of freedom. Disturbances to an unstable, nonlinear wave-mean oscillation are analyzed, allowing the comparison of singular vectors and time-dependent normal modes (Floquet vectors). Singular vectors characterize the transient growth of linear disturbances in a specified inner product over a specified time interval and, as such, they complement and are related to Lyapunov vectors, which characterize the asymptotic growth of linear disturbances. The relationship between singular vectors and Floquet vectors (the analog of Lyapunov vectors for time-periodic systems) is analyzed in the context of a nonlinear baroclinic wave-mean oscillation. It is found that the singular vectors divide into two dynamical classes that are related to those of the Floquet vectors. Singular vectors in the "wave dynamical" class are found to asymptotically approach constant linear combinations of Floquet vectors. The most rapidly decaying singular vectors project strongly onto the most rapidly decaying Floquet vectors. In contrast, the leading singular vectors project strongly onto the leading adjoint Floquet vectors. Examination of trajectories that are near the basic cycle show that the leading Floquet vectors are geometrically tangent to the local attractor while the leading initial singular vectors point off the local attractor. A method for recovering the leading Floquet vectors from a small number of singular vectors is additionally demonstrated.

1. Introduction

Geophysical flows are continually subjected to disturbances that may cause them to evolve away from their previously observed or expected states. An understanding of the evolution of disturbances to geophysical flows is necessary if these flows are to be predicted. Classical studies of disturbance growth, encompassing the well-known normal-mode instability theories of fluid dynamics, concentrated on the asymptotic development of disturbances to idealized flows. Since the development of operational numerical forecasting, increasing attention has focused on the transient development of disturbances. For flows with complex time dependence, however, the distinction between asymptotic and transient stability is often not clear. For example, many forced–dissipative flows evolve toward aperiodic attractors where all trajectories are asymptotically unstable, yet disturbances to these trajectories may go through periods of dramatic transient growth and decay.

The transient development of disturbances is typically quantified using singular values and their associated singular vectors (SVs). Singular vectors are disturbances that produce the greatest linear growth in a specified inner product over a specified optimization time interval (Lorenz 1965; Farrell 1989). There is considerable arbitrariness in the choice of an inner product and optimization interval, which can make their physical interpretation difficult.

The asymptotic stability of trajectories on aperiodic attractors is described by Lyapunov exponents, which give the average growth rate of volume elements in the attractor. Lyapunov vectors (LVs) are physical structures associated with the Lyapunov exponents. Since Lyapunov exponents naturally generalize the stability exponents of normal modes to aperiodic systems, it might be hoped that a suitable definition of the LVs will

* Current affiliation: Scripps Institution of Oceanography, University of California, San Diego, La Jolla, California.

Corresponding author address: Christopher L. Wolfe, Scripps Institution of Oceanography, University of California, San Diego, 9500 Gilman Dr., La Jolla, CA 92093-0213.
E-mail: clwolfe@ucsd.edu

naturally generalize normal modes to aperiodic flows. Also, since the unstable LVs exhibit the largest disturbance growth in the long term, it might be hoped that initializing ensemble forecasting systems with LVs will also lead to largest ensemble spread in the long term, maximizing the utility of the forecast system. The different requirements of these two applications have lead to different definitions of the LVs. We use a definition of the LVs, established by Ruelle (1979) and introduced into the meteorological literature by Legras and Vautard (1996, who call them characteristic vectors) and Trevisan and Pancotti (1998), that satisfies the Oseledec (1968) theorem. In contrast to SVs, the LVs so defined are independent of norm and optimization time, invariant under the linearized dynamics, generally nonorthogonal, and can be shown to be a proper generalization of normal modes to aperiodic flows (Trevisan and Pancotti 1998; Wolfe and Samelson 2007). These LVs often undergo significant transient growth and decay in addition to their asymptotic, exponential evolution.

Both SVs and an analog of LVs, bred vectors, are currently in use at operational forecasting centers as initial conditions for ensemble forecasting systems (Buizza et al. 2005). Bred vectors are generated through a repeated "breeding" cycle by which the differences between the analysis and the ensemble members are rescaled and added back to the analysis to generate a new set of ensemble initial conditions (Toth and Kalnay 1993, 1997). Since the ensemble forecast models are nonlinear, bred vectors of sufficient magnitude are nonlinear disturbances. If the amplitude of the bred vectors is constrained so that the disturbances remain linear, the process by which bred vectors are generated is analogous to the methods used to estimate the Lyapunov exponents of dynamical systems (Shimada and Nagashima 1979).

In the present contribution, we examine the relationships between SVs and LVs and the relationship of both to the local structure of the system's attractor. The relationship between these quantities is of interest not only because of the connections to ensemble forecasting, but also because Lyapunov exponents and vectors are intrinsic, asymptotic properties of a dynamical system's attractor, whereas singular values and vectors depend both on the choice of inner product and the time interval of interest. The connection between transient and asymptotic stability in strongly time-dependent systems has primarily been studied using either highly simplified, low-order models (e.g., Lorenz 1965; Trevisan and Pancotti 1998; Samelson 2001b) or models with complexity comparable to global circulation models (e.g., Buizza and Palmer 1995; Palmer 1996; Wei and

Frederiksen 2004). Examples of accessible, intermediate complexity models are few (with exceptions; see, e.g., Samelson and Tziperman 2001; Miller and Ehret 2002; Stevens and Hakim 2005). One goal of the present contribution is to present an accessible system wherein the relationships between asymptotic and transient stability may be examined in detail.

It should be noted that the majority of the studies that examine the relationship between SVs and LVs either use an orthogonalized LV (Vastano and Moser 1991; Vannitsem and Nicolis 1997; Reynolds and Errico 1999) or focus only on the leading LV (Szunyogh et al. 1997; Samelson 2001a). The former case presents difficulties with interpretation since orthogonalized LVs are essentially identical to SVs with asymptotically long optimization intervals (Trevisan and Pancotti 1998). Indeed, some authors (Legras and Vautard 1996; Reynolds and Errico 1999) define the LVs to be *precisely* SVs with asymptotically long optimization intervals. Thus, studies comparing SVs to orthogonalized LVs are more properly thought of as comparing SVs with finite optimization intervals to SVs with asymptotically long optimization intervals. Studies that focus on a single leading LV do not present any difficulties with interpretation, but may be misleading in systems with multiple unstable LVs.

The system under study is a strongly nonlinear, chaotic solution to the nonlinear Phillips (1954) model. This model is chosen because it is relatively well understood and occupies a middle ground in complexity between the low-dimensional models used in classical predictability studies and operational forecast models. The intermediate complexity of the model allows the representation of nontrivial physics while still admitting a relatively complete analysis.

Most of the present analysis focuses on a single unstable, nonlinear, time-periodic oscillation (cycle) of the model. Periodic cycles are convenient because full information about the evolution of linear disturbances can be obtained by a single integration over the cycle. Additionally, time periodicity imposes a definite modal structure on the linear space tangent to the cycle in the form of Floquet vectors (FVs). Further, LVs reduce to FVs for time-periodic flows (Trevisan and Pancotti 1998; Wolfe and Samelson 2007). Floquet vectors may thus be unambiguously identified as both normal modes and LVs. The wave-mean oscillation that will be considered here and the associated FVs are described in detail in Wolfe and Samelson (2006, hereafter WS), which should be considered a companion to the present contribution.

The present study may be thought of as an extension of the studies of Samelson (2001a,b), who considered

LVs and SVs in a weakly nonlinear, weakly chaotic regime of the model considered here. One of the most striking conclusions of these studies was that the representations of SVs in terms of the LVs were relatively simple functions of time, even though both are individually strongly time dependent. The present study finds similar results, albeit complicated by the increase in the complexity of the model and its dynamics.

The format of the paper is as follows: In section 2, we briefly describe the model, basic cycle, and normal modes used for the present analysis, as well as the basic properties of LVs and SVs. Section 3 is devoted to a detailed discussion of the SVs and their relationship to the FVs. In section 4, we examine the relationship of the FVs and SVs to the local structure of the system's attractor. A method for recovering the FVs from the SVs is described and demonstrated in section 5. The significance of the results is discussed in section 6. Finally, we summarize in section 7.

2. Formulation

a. Model and basic cycle

The model studied here is the nonlinear Phillips (1954) quasigeostrophic channel model, which is described in detail in Pedlosky (1987, section 7). For the present study, the Coriolis parameter f is constant, the equilibrium layer depths are equal, and the background flow is steady, uniform, and zonal. The model equations were solved in the manner described in WS except that the Adams–Bashforth three-level time-differencing scheme was used throughout. Also, since the SV calculation is numerically more stable than the Floquet problem, we were able to use a slightly lower resolution than WS. Thus, the results of the present study were obtained using $N_x = 48$ zonal and $N_y = 40$ meridional grid points, for a total of 3840 variables, and a time step of $\Delta t = 0.0015$.

The two parameters controlling the behavior of the system are the Froude number F and the Ekman dissipation parameter r. In the notation of Klein and Pedlosky (1986), we use

$$\Delta \equiv F - \pi^2 - 4r^2 = 45, \quad \gamma \equiv r\sqrt{8/\Delta} = 0.20,$$

which corresponds to the most strongly supercritical set of parameters considered by Klein and Pedlosky (1986). For these parameters the system possesses an aperiodic attractor with Kaplan–Yorke (Lyapunov) dimension >7. The basic cycle considered here is an unstable periodic orbit embedded in this attractor. It has a period of $T \approx 38.498$ and begins as a nearly zonal flow with a small superimposed perturbation. This perturba-

tion grows into a pair of eddies that grow in amplitude as they advect heat (proportional to $\psi_T = \psi_1 - \psi_2$) downgradient, across the channel. By $t = 0.3T$, these eddies are strongly nonlinear and have closed streamfunction contours. The cross-channel heat flux produced by these eddies reduces the background potential vorticity gradient sufficiently to halt and then reverse the growth of the eddies. Toward the end of the decay phase, the weakening eddies advect heat upgradient, extracting energy from the wave and reestablishing the nearly zonal initial state, now shifted downchannel by one-half the channel length. After passing through a second growth and decay phase, the flow returns to its initial state. The basic cycle is described in more detail in WS.

The period of the basic cycle is much longer than either the advective or viscous time scales:

$$T_a = \frac{1}{U_{\max}} \approx 0.02T; \quad T_\nu = \frac{1}{r} \approx 0.05T,$$

respectively. Since the basic cycle undergoes two growth and decay episodes in each period, the characteristic time scale for baroclinic wave growth is

$$T_w \approx 0.25T.$$

Based on the above scales, we expect advective alignment of disturbances to be important only on extremely short time scales. Baroclinic processes related to the growth and maintenance of the basic cycle are expected to dominate disturbance growth for moderate to long time scales.

In principle, the basic cycle is the first in an infinite series of unstable periodic cycles with progressively longer periods that form a "skeleton" for the aperiodic attractor, and any quantity defined on the attractor may be recovered by forming suitable sums over the unstable periodic cycles (e.g., Cvitanović et al. 2005). In practice, long unstable periodic cycles are very hard to find in high-dimensional systems. Fortunately, the sums involved are given with exponential accuracy by the low-period cycles (Lai et al. 1997) and useful results may often be obtained using just a few low-period cycles (Kazantsev 1998, 2001). As discussed in WS, the basic cycle captures many of the features of the system's aperiodic attractor. In particular, the Lyapunov spectrum of the basic cycle is very similar to that of the attractor. The calculations have been repeated using a few higher period cycles and at different parameter settings with little change in the qualitative features of the results.

b. Lyapunov vectors and Floquet vectors

The LVs ϕ_i are the physical structures associated with the Lyapunov exponents λ_i, which are ordered by

increasing stability. A norm-independent set of LVs ϕ_i may be defined using the following consequence of the Oseledec (1968) theorem: For almost every time t, there exists two sets of nested subspaces

$$\mathcal{S}_M^+(t) \subset \mathcal{S}_{M-1}^+(t) \subset \cdots \subset \mathcal{S}_1^+(t) = \mathbb{R}^N \qquad (1)$$

and

$$\mathcal{S}_M^-(t) \subset \mathcal{S}_{M-1}^-(t) \subset \cdots \subset \mathcal{S}_1^-(t) = \mathbb{R}^N, \qquad (2)$$

such than any vector $\mathbf{y} \in \mathcal{S}_i^\pm(t) \backslash \mathcal{S}_{i+1}^\pm(t)$ grows asymptotically at the rate $\pm \hat{\lambda}_i$, where $\hat{\lambda}_i$ is the ith *distinct* Lyapunov exponent and $M \leq N$ is the number of distinct Lyapunov exponents (Ruelle 1979). The intersection space

$$\mathcal{T}_i(t) = \mathcal{S}_i^+(t) \cap \mathcal{S}_{M-i+1}^-(t) \qquad (3)$$

is, in general, m_i dimensional, where m_i is the multiplicity of the ith Lyapunov exponent. If $d = 1$, then $\mathcal{T}_i$ may be identified as the LV ϕ_i since it grows asymptotically at the rates $\hat{\lambda}_i$ and $-\hat{\lambda}_i$ as the system evolved forward and backward, respectively, in time. If $d > 1$, then any m_i linearly independent vectors from $\mathcal{T}_i$ may be identified as LVs.

The ϕ_i defined in this manner are norm independent and characterize the asymptotic stability of linear disturbances as the system evolves both forward and backward in time. Further, the ϕ_i reduce to the FVs if the flow is time periodic (Trevisan and Pancotti 1998) and to the stationary normal modes if the flow is stationary. Finally, the ϕ_i are invariant under the linearized flow, in the sense that they may, in principle, be computed once and then determined for all time using the tangent linear propagator.

In the present case, the background flow is time periodic and the LVs reduce to FVs, which may be calculated as the eigenvectors of the one-period linear disturbance propagator $\mathcal{L}(T)$, where the propagator satisfies

$$\boldsymbol{\xi}(t + T) = \mathcal{L}(T)\boldsymbol{\xi}(t) \qquad (4)$$

for any time t and any linear disturbance $\boldsymbol{\xi}(t)$ (Coddington and Levinson 1955). In the present case, three of the FVs are unstable and two are neutral, indicating that the basic cycle has multiple normal-mode instabilities. The number of unstable and neutral modes is independent of resolution and is an intrinsic characteristic of the basic cycle. The rest of the Floquet spectrum is completed by a large number of decaying modes, the exact number of which depends on resolution.

The exponential growth of the unstable FVs is relatively slow, with e-folding times of

$$T_1 \approx 0.9T, \quad T_2 \approx 1.2T, \quad T_3 \approx 3.6T,$$

for the first, second, and third FVs, respectively. While these time scales are longer than the transient baroclinic wave growth time scale T_w, the leading FVs undergo significant transient growth and decay in phase with the basic cycle. The maximum transient growth rate of the unstable FVs is inner product dependent, but is on average about 10 times faster than the exponential growth rate in most physically motivated inner products.

A striking feature of the Floquet spectrum is that the FVs split into two distinct dynamical classes. The FVs in the "wave dynamical" (WD) class have growth/decay rates that are well separated from the dissipation rate and have spatial structures that are dominated by a few large-scale Fourier components. In contrast, FVs in the "damped advective" (DA) class are characterized by fine scales, broad Fourier spectrums, and decay rates near the dissipation rate. The naming scheme reflects the primary dynamical balances of the FVs in each class: WD modes grow and decay due to baroclinic wave dynamics, while the DA modes are simply advected by the mean flow and dissipated by Ekman friction. The WD modes tend to be frequency locked to the basic cycle and thus have real Floquet exponents, while DA modes have complex Floquet exponents with imaginary parts that are distributed approximately uniformly between $\pm\pi/T$ and thus either have very long periods or are quasiperiodic. Further, the number of WD modes is only weakly dependent on resolution and their physical structures become independent of resolution once the model is sufficiently well resolved. The number of DA modes, in contrast, increases apparently without limit as the model resolution is increased and individual DAs appear to change discontinuously with resolution. These features lead WS to speculate that the WD modes represent true, discrete dynamical modes, while the DA modes are best thought of as representing, in sum, a generalized solution to the damped-advective problem, which, in the continuum limit, may support a continuous spectrum of modes. Due to the difficulty of assigning physical interpretations to individual DA modes, the focus of the present contribution will be on the comparison of singular vectors to the WD modes, which comprise both growing/weakly decaying modes and the most rapidly decaying modes.

An important property of these FVs from the point of optimal disturbances (singular vectors) is that they are nonorthogonal in the inner products considered in

section 3. This follows from the fact that the one-period propagator $\mathcal{L}(T)$ is nonnormal [i.e., it does not commute with its adjoint $\mathcal{L}(T)^{\dagger}$ in these inner products]. A further consequence of the nonnormality of $\mathcal{L}(T)$ is that the adjoint FV $\boldsymbol{\theta}_i$, the eigenvectors of the adjoint propagator, are distinct from the "forward" FV ϕ_i. The $\boldsymbol{\theta}_i$ are nonorthogonal, as well, but can be ordered so that they satisfy the following orthogonality relationship with the ϕ_i:

$$\langle \boldsymbol{\theta}_i, \phi_j \rangle = \Pi_{ij}^{-1} \delta_{ij}, \tag{5}$$

where $\boldsymbol{\Pi}$ is a diagonal matrix whose nonzero entries are the "projectabilities" of the adjoint FVs onto the forward FVs [Stoer and Bulirsch (2002); the term projectability is due to Zhang (1988)].

If the chosen inner product $\langle \cdot, \cdot \rangle$ is characterized by the matrix $\mathbf{N}$ such that $\langle \mathbf{v}, \mathbf{w} \rangle = \mathbf{v}^{\mathrm{T}} \mathbf{N} \mathbf{w}$, then the adjoint propagator satisfies $\mathbf{N}\mathcal{L}(T)^{\dagger} = \mathcal{L}(T)^{\mathrm{T}} \mathbf{N}$. Equation (5) may then be inverted to define the $\boldsymbol{\theta}_i$ in terms of the ϕ_i:

$$\mathbf{T} = \mathbf{N}^{-1} \mathbf{F}^{-\mathrm{T}} \boldsymbol{\Pi}^{-1}, \tag{6}$$

where $\mathbf{T}$ and $\mathbf{F}$ are matrices whose columns are the $\boldsymbol{\theta}_i$ and ϕ_i, respectively. While matrix inversion is not necessarily more efficient then eigenvalue decomposition, computation of the adjoint FVs via (6) ensures that they are automatically sorted in the same manner as the forward FVs (i.e., by increasing stability).

The primary property of the $\boldsymbol{\theta}_i$ that will be of use in the present study is that, for large optimization times, the adjoint FV $\boldsymbol{\theta}_i$ is the optimal excitation of ϕ_i with respect to the inner product defining the adjoint. [Farrell (1989) and Buizza and Palmer (1995) demonstrate this fact for stationary flows. The extension to time-periodic flows is straightforward.] That is, $\boldsymbol{\theta}_i$ is the smallest perturbation at time t_0 that will produce an excitation of ϕ_i at unit amplitude at a later time t_1.

c. Singular vectors

SVs optimize the growth of perturbations in a specified inner product over a specified optimization interval $\tau = t_1 - t_0$. Let $\boldsymbol{\xi}_j(t)$ represent the jth most rapidly growing SV. Since the FVs span the space of linear disturbances, $\boldsymbol{\xi}_j(t)$ may be written as a fixed sum of FVs:

$$\boldsymbol{\xi}_j(t) = \sum_{i=1}^{N} \phi_i(t) p_{ij} = \mathbf{F}(t)\mathbf{p}_j. \tag{7}$$

The projection coefficients $\mathbf{p}_j$ are independent of time, so, if the $\phi_i(t)$ are known, $\boldsymbol{\xi}_j(t)$ is determined for all time. The SV optimization problem leads, in the usual way (e.g., Buizza et al. 1993), to the generalized eigenvalue problem:

$$\mathbf{F}(t_1)^{\mathrm{T}} \mathbf{N} \mathbf{F}(t_1) \mathbf{p}_j = \sigma_j^2 \mathbf{F}(t_0)^{\mathrm{T}} \mathbf{N} \mathbf{F}(t_0) \mathbf{p}_j \tag{8}$$

for the SVs and the singular values σ_j, where $\mathbf{N}$ is the matrix that characterizes the specified inner product. Note that the $\mathbf{p}_j$ are not invariant under an arbitrary rescaling of the FVs: in what follows, we have chosen the FVs to have unit amplitude in the specified norm at the initialization time t_0.

The SV $\boldsymbol{\xi}_j$ may equivalently be written as a fixed sum of adjoint FVs $\boldsymbol{\theta}_i(t)$:

$$\boldsymbol{\xi}_j(t) = \sum_{i=1}^{N} \boldsymbol{\theta}_i(t) q_{ij} = \mathbf{T}(t)\mathbf{q}_j, \tag{9}$$

where the $\mathbf{q}_j$ are the adjoint projection coefficients. Such an expansion is useful since, for large optimization intervals, the optimal excitation of the normal mode ϕ_i is the corresponding adjoint normal mode $\boldsymbol{\theta}_i$ (Farrell 1989; Buizza and Palmer 1995). The $\mathbf{q}_j$ satisfy the generalized eigenvalue problem

$$\mathbf{T}(t_1)^{\mathrm{T}} \mathbf{N} \mathbf{T}(t_1) \mathbf{q}_j = \sigma_j^{-2} \mathbf{T}(t_0)^{\mathrm{T}} \mathbf{N} \mathbf{T}(t_0) \mathbf{q}_j, \tag{10}$$

but if—as in the present case—the complete set of FVs is available, the $\mathbf{q}_j$ may be more efficiently computed using

$$\mathbf{q}_j = \mathbf{T}(t_0)^{-1} \mathbf{F}(t_0) \mathbf{p}_j = \boldsymbol{\Pi} \mathbf{F}(t_0)^{\mathrm{T}} \mathbf{N} \mathbf{F}(t_0) \mathbf{p}_j, \tag{11}$$

where the last equality follows from (6). Note that the rhs of (11) is merely the rhs of (8) weighted by the projectability factors $\boldsymbol{\Pi}$.

The SVs depend on the initialization and optimization times t_0 and t_1 as well as on the inner products defined by the matrix $\mathbf{N}$. We have calculated SVs using inner products $\langle \cdot, \cdot \rangle$ corresponding to the streamfunction variance (SA), wave energy (WE), and potential enstrophy (PV). These inner products are defined as follows:

$$\langle \mathbf{v}, \mathbf{w} \rangle_{\mathrm{SA}} = \sum_{n=1}^{2} \iint \psi_n^{(\mathbf{v})} \psi_n^{(\mathbf{w})} \, dx \, dy, \tag{12}$$

$$\langle \mathbf{v}, \mathbf{w} \rangle_{\mathrm{WE}} = \sum_{n=1}^{2} \frac{1}{2} \iint \boldsymbol{\nabla}\psi_n^{(\mathbf{v})} \cdot \boldsymbol{\nabla}\psi_n^{(\mathbf{w})} \, dx \, dy$$
$$+ \frac{F}{2} \iint [\psi_1^{(\mathbf{v})} - \psi_2^{(\mathbf{v})}][\psi_1^{(\mathbf{w})} - \psi_2^{(\mathbf{w})}] \, dx \, dy, \tag{13}$$

$$\langle \mathbf{v}, \mathbf{w} \rangle_{\mathrm{PV}} = \sum_{n=1}^{2} \iint q_n^{(\mathbf{v})} q_n^{(\mathbf{w})} \, dx \, dy, \tag{14}$$

where $\psi^{(\mathbf{v},\mathbf{w})}$ and $q^{(\mathbf{v},\mathbf{w})}$ denote the disturbance streamfunction and potential vorticity associated with the dis-

turbance state vectors **v** and **w** and the integrals are taken over the entire domain. While SVs were calculated in all three inner products, the bulk of the discussion will focus on the SVs computed in the WE inner product, with comments on the SA and PV SVs only when their behavior differs significantly from the WE SVs. This focus on the WE SVs is reasonable both because they typically show behavior that is intermediate between the SA and PV SVs and because the WE inner product is the analog, in the Phillips model, of the "total energy" inner product commonly used to compute singular vectors in atmospheric global circulation models (Buizza and Palmer 1995; Palmer 1996).

3. The relationship of singular vectors to Lyapunov vectors

Here we examine the relationship between singular vectors and Lyapunov vectors using Floquet decompositions of the singular vectors, as discussed in section 2c. The behavior of the decompositions as both the SV initialization time t_0 and optimization interval τ are varied is investigated by computing SVs with fixed t_0, but variable τ, and with fixed τ, but variable t_0. The eigenvalue problem Eq. (8) for the SVs yields as many SVs as model variables (in this case, 3840). A subset of the calculations was repeated at higher resolution with little change in the structure of the extremal (i.e., most rapidly growing and decaying) SVs. The SVs in the middle of the spectrum—which are not the focus of the present contribution—changed in number and detailed physical structure with changes in resolution, but their overall statistical character remained the same. See WS for a detailed discussion of the effects of resolution on the structure of linear disturbances to the basic cycle.

The singular values computed with initialization time t_0 fixed at a basic cycle minimum undergo a short period of super-Lyapunov (i.e., faster than the exponential growth rate of the FVs) growth and decay for short optimization intervals (Fig. 1). The rapid transient growth period is more pronounced in the SA inner product than in the WE inner product, while the SVs in the WE inner product similarly undergo more transient growth than the SVs in the PV inner product. In all cases, the growth rates of the singular values becomes comparable to the effective exponential growth rate of the FVs,

$$\lambda_{\text{eff},j}(t_2) = \frac{1}{t_2 - t_1} \ln \frac{\|\phi_j(t_2)\|}{\|\phi_j(t_1)\|}, \qquad (15)$$

for optimization intervals greater than a few advective time scales T_a, or roughly one baroclinic growth time
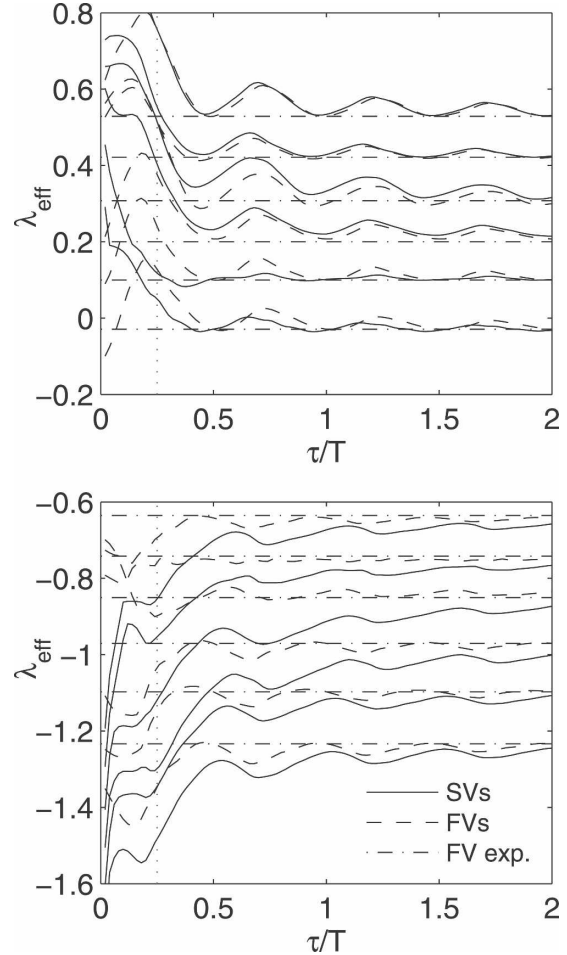

FIG. 1. Effective exponential growth rate λ_{eff} of the (top) first and (bottom) last five SVs (solid) and FVs (dashed) in the WE norm, as well as the respective Floquet exponents (dash–dot) as a function of optimization interval τ/T. The vertical lines give the time $t = T_w$. The growth rates have been offset from each other by 0.1 for clarity. The least rapidly (top) growing and (bottom) decaying vectors have zero offset.

scale $T_w \approx 0.25T$ (Fig. 1). Further, the growth rates of the SVs asymptotically approach the Floquet exponents as the optimization interval τ increases.

Once $\tau \gtrsim T_w$, the SVs in each inner product divide into two classes, much like the FVs. The first class, which may be identified with the WD class, is made up of vectors whose singular values either grow or decay at rates that are significantly different than the dissipation rate. The second class is made up of a large number of SVs that decay at or near the dissipation rate, and SVs may be identified with the DA class. The WD singular values show pronounced oscillations on the time scale of the basic cycle wave growth time scale T_w (Fig. 2). These oscillations are in phase with the basic cycle in
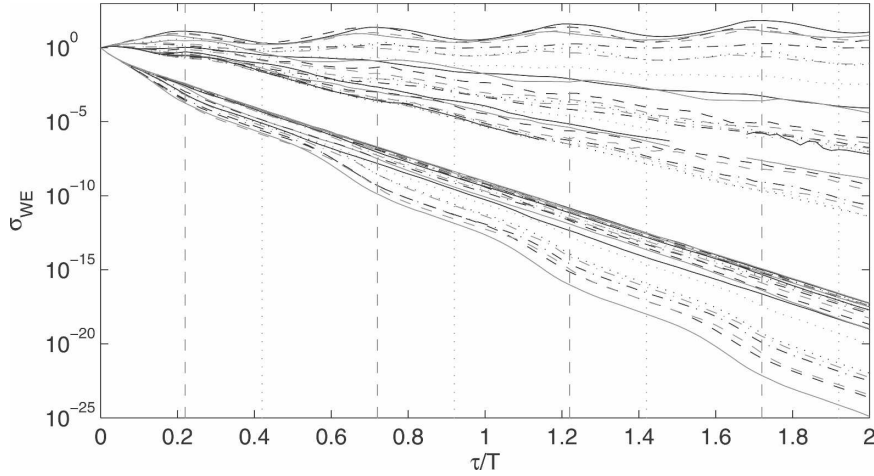
FIG. 2. Singular values in the WE inner product vs optimization interval τ/T for fixed initialization time t_0 near a basic cycle minimum. For clarity, only the the first and last 25 singular values are shown. Some of the singular values did not converge at large optimization times; these values are omitted. The maxima and minima of the basic cycle are denoted by the vertical dashed and dotted lines, respectively.

the SA inner product, but slightly trail the basic cycle in the WE and PV inner product. This difference is most likely due to the fact that energy and PV disturbances continue to sharpen during the early parts of the basic cycle decay phase.

While the WD singular values are well separated relative to the DA singular values, the separation is not perfect and the SVs exchange stability frequently, which makes the ranking of the SVs ambiguous. For this section, the numerical ranking of the SVs is based on the ranking of the corresponding singular values at the largest optimization interval considered ($\tau = 2T$). Thus, $\boldsymbol{\xi}_1$ is the leading SV at time $\tau = 2T$ but, since the SVs exchange stability as the optimization interval is changed, $\boldsymbol{\xi}_1$ may not be the leading SV for $\tau < 2T$. Since the physical structures of the SVs change continuously as the optimization interval is varied, the individual SVs may be consistently identified even if the singular values cross.

The leading WE SVs show significant contributions from a large number of FVs (not shown). The largest contributions often come from weakly decaying WD FVs or from DA FVs, while the leading FVs are typically subdominant. By contrast, the leading SVs are relatively simple functions of a small number of the adjoint FVs (Fig. 3). In fact, for $\tau \gtrsim 2T_w$, the leading SVs are nearly optimal excitations of the leading FVs. Thus, by the optimization time, the leading SVs will be nearly collinear with the leading FVs. Note that both $\boldsymbol{\xi}_2$ and $\boldsymbol{\xi}_5$ (respectively, $\boldsymbol{\xi}_4$ and $\boldsymbol{\xi}_6$) have large projections onto $\boldsymbol{\theta}_2$ and $\boldsymbol{\theta}_4$ (respectively, $\boldsymbol{\theta}_3$ and $\boldsymbol{\theta}_6$), but the roles of the adjoint FVs are reversed. This occurs because $\boldsymbol{\theta}_2$

and $\boldsymbol{\theta}_4$ (respectively, $\boldsymbol{\theta}_3$ and $\boldsymbol{\theta}_6$) are orthogonal, or nearly so, in all three inner products, to all of the leading adjoint FVs except each other.

For optimization intervals $\tau \gtrsim 2T_w$, the most rapidly damped SVs project onto only the most rapidly damped FVs (Fig. 4). This is a consequence of the optimization problem that defines the SVs: the most rapidly damped SVs can only project onto the most rapidly damped FVs since, if they did not, they would decay less rapidly. As with the leading SVs, the FV components of the most rapidly decaying SVs tend to occur in alternating pairs due to the fact that the FV pairs $\phi_{3835,3839}$, $\phi_{3836,3840}$, and $\phi_{3837,3838}$ are orthogonal (to within numerical precision), in all three inner products, to all other rapidly decaying FVs except each other.

Both the leading and most rapidly decaying SVs appear to be converging to constant linear combinations of FVs as τ increases for all inner products considered (3 and 4). The rate of convergence, however, is different for different SVs, and $\boldsymbol{\xi}_4$ and $\boldsymbol{\xi}_5$ still show marked oscillations in their (adjoint) FV decompositions for the largest optimization intervals shown. It may be shown that the SVs converge exponentially, at a rate which may be estimated from the Floquet exponents, to orthogonalizations of the FVs as the optimization time $|\tau| \to \infty$ (Wolfe and Samelson 2007). This will be explored more fully in section 5.

The rapid convergence of the growing (respectively, decaying) SVs to constant linear combinations of a small number of adjoints (respectively, forward) is not a special consequence of the choice of the cycle minimum as the initialization time. This can be seen by
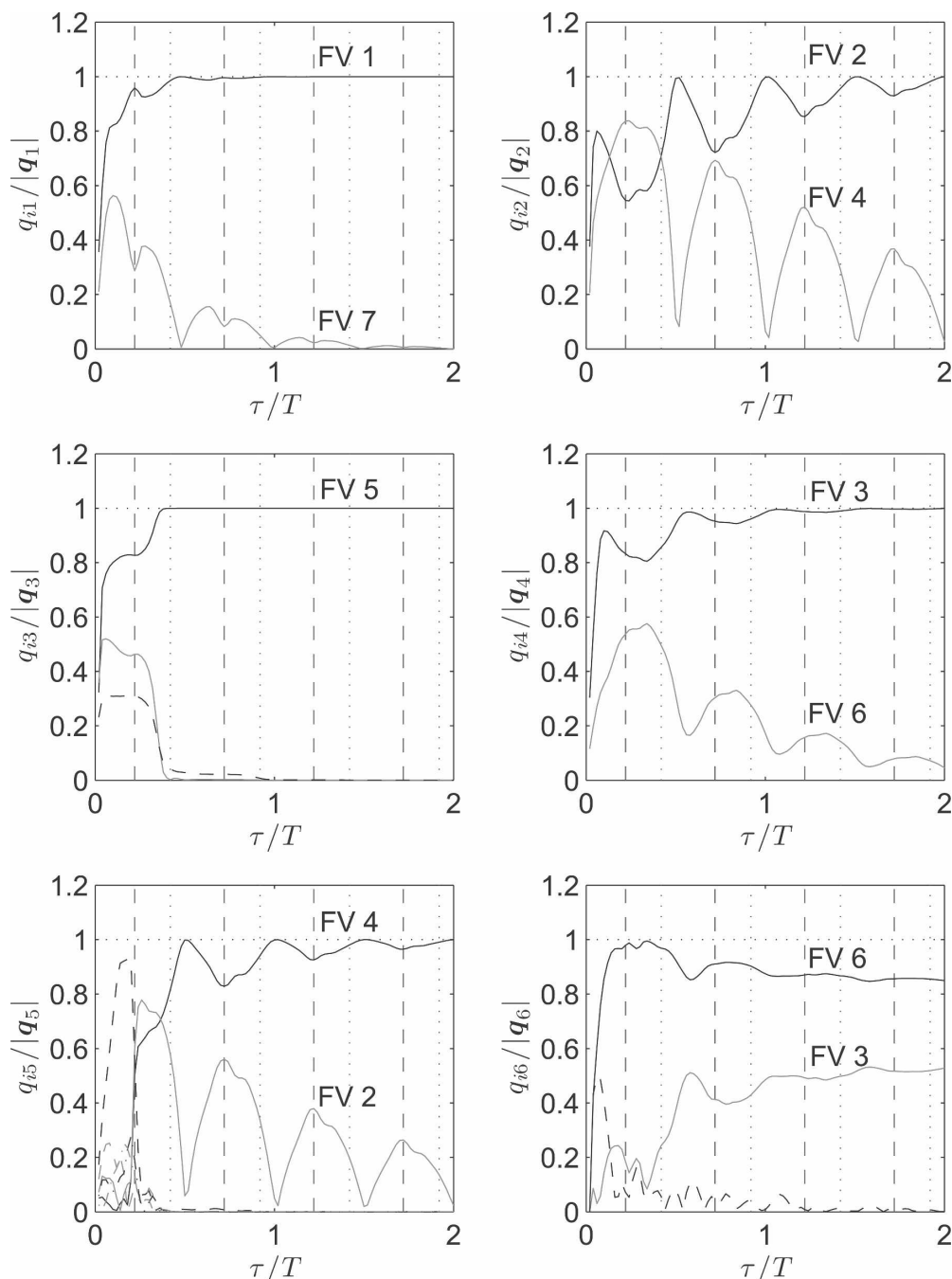
FIG. 3. Magnitude of the adjoint FV components $\mathbf{q}_j$ of the leading SVs' $\boldsymbol{\xi}_j$ in the WE inner product vs optimization interval τ/T for fixed initialization time t_1. Components always less than 0.2 have been omitted for clarity and the Floquet indices of the dominant components are noted in each plot. The vertical lines are as in Fig. 2.

considering the Floquet decompositions of the SVs as a function of initialization time with the optimization interval fixed to $\tau = T$. Again, the leading SVs are relatively simple functions of a small number of the adjoint FVs (Fig. 5). For each initialization time, the leading

five SVs are nearly optimal excitations of the *same* FVs. Both $\boldsymbol{\xi}_2$ and $\boldsymbol{\xi}_5$ (respectively, $\boldsymbol{\xi}_4$ and $\boldsymbol{\xi}_6$) have large projections onto $\boldsymbol{\theta}_1$ and $\boldsymbol{\theta}_7$ (respectively, $\boldsymbol{\theta}_2$ and $\boldsymbol{\theta}_4$), but the roles of the adjoint FVs are reversed. As in the previous case, this occurs because $\boldsymbol{\theta}_1$ and $\boldsymbol{\theta}_7$ (respectively, $\boldsymbol{\theta}_2$ and
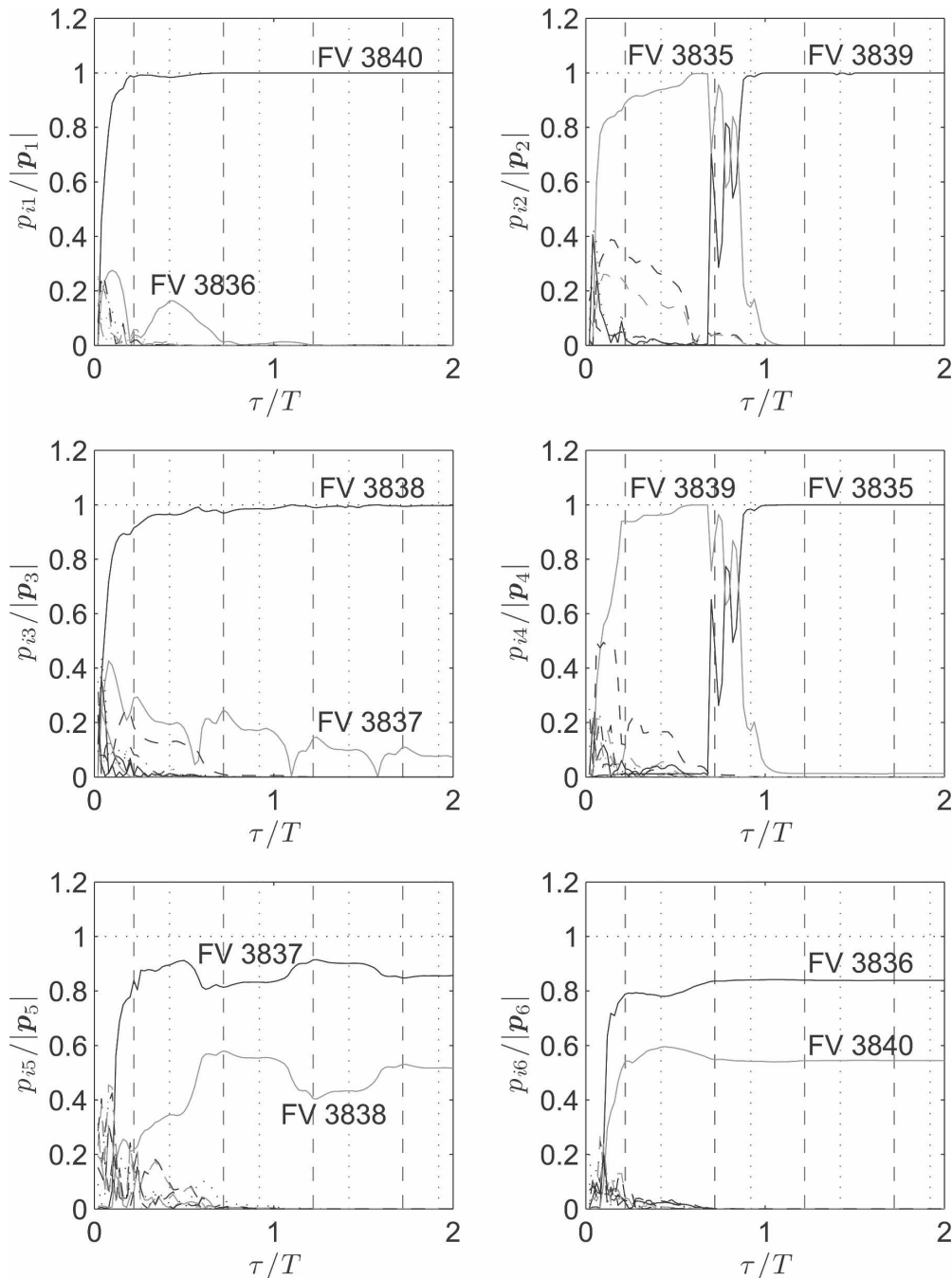
FIG. 4. As in Fig. 3 but for the magnitude of the FV components $\mathbf{p}_j$ of the most rapidly decaying SV $\boldsymbol{\xi}_j$.

$\boldsymbol{\theta}_4$) are orthogonal, in all three inner products, to all of the leading adjoint FVs except each other. Similarly, the most rapidly decaying SVs project onto the same FVs, regardless of initialization time (Fig. 6). Both $\boldsymbol{\xi}_{3836}$ and $\boldsymbol{\xi}_{3838}$ project strongly onto the same FVs, but with their roles exchanged.

If the optimization interval is reduced to $\tau = T_w$, the modal structure is not as clear as those at longer opti-

mization intervals. However, the leading SVs are still relatively simple functions of a few adjoint FVs (Fig. 7), although a larger number of adjoint FVs have more significant magnitude than with $\tau = T$. The most rapidly decaying SVs (not shown), by contrast, have a large number of components of roughly equal magnitude, which are complicated functions of initialization time. This suggests that the leading SVs converge more
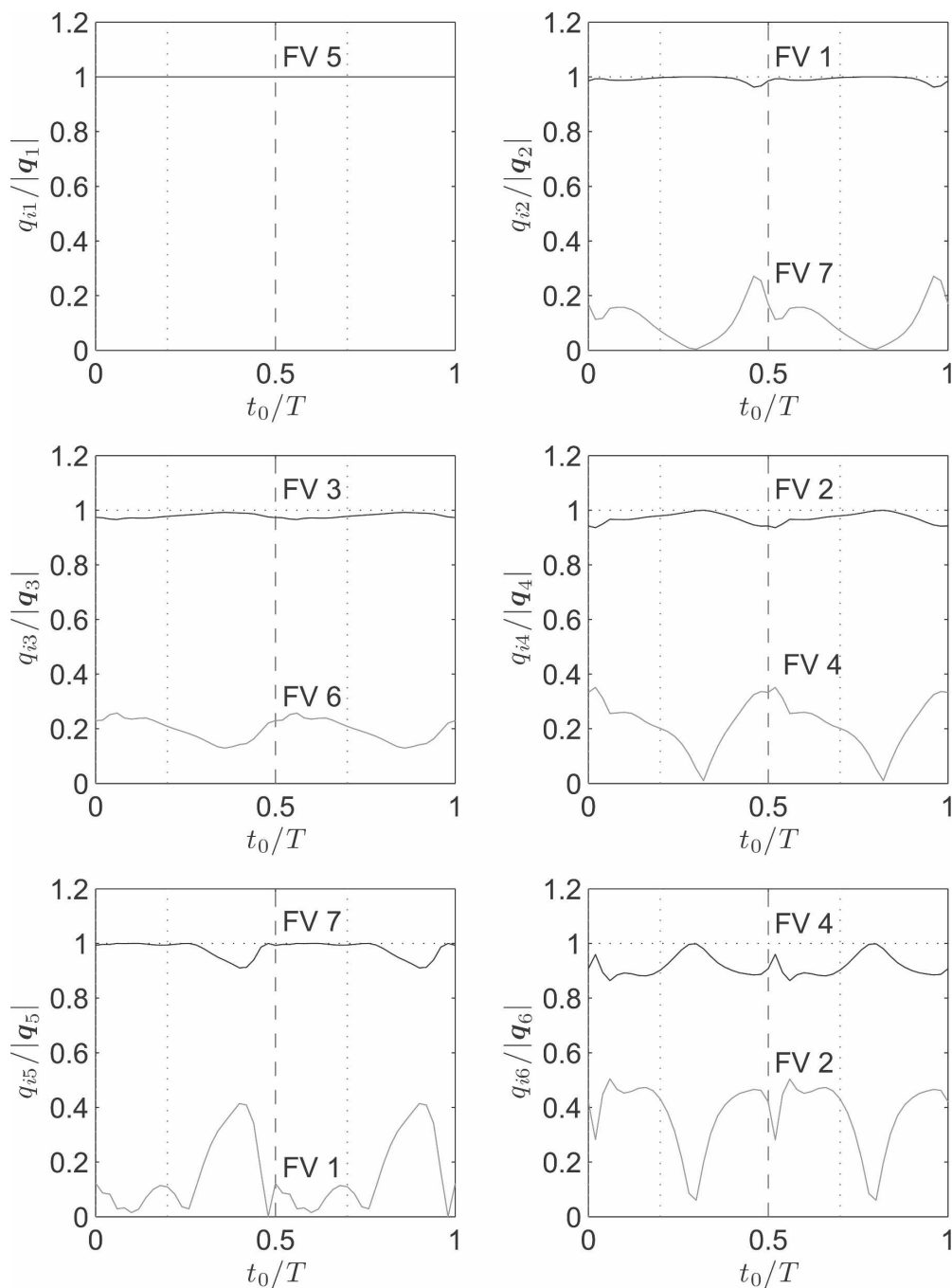
FIG. 5. Magnitude of the adjoint FV components $\mathbf{q}_j$ of the leading SVs in the WE inner product vs initialization time t_0/T for fixed optimization interval $\tau = T$. Components always less than 0.2 have been omitted for clarity. The vertical lines are as in Fig. 2.

quickly than the rapidly decaying SVs, and one baro-clinic growth cycle is not sufficiently long to allow these SVs to converge to their asymptotic form.

The Floquet decompositions of the SVs in the other two inner products are qualitatively similar. The primary difference is that, as the number of derivatives in the inner product decreases, the number of FVs contributing significantly to each SV increases. This is due to the fact that the FVs themselves become closer to orthogonal as the number of derivatives in the inner product increases.

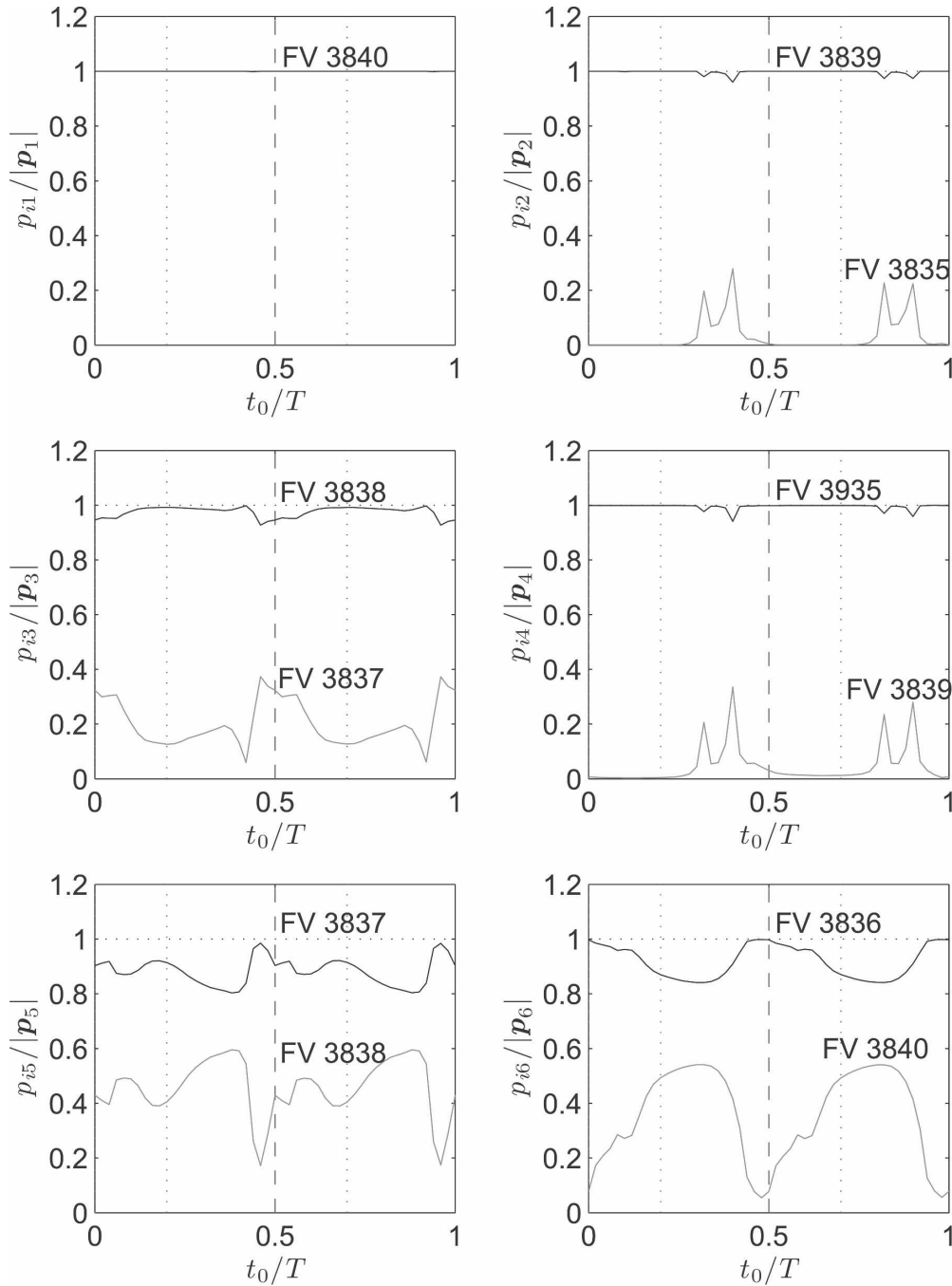While the Floquet decompositions of the SVs calcu-

FIG. 6. As in Fig. 5 but for the most rapidly decaying SVs.

lated in the three inner products are qualitatively similar, the temporal evolution of their spatial scales is remarkably different. The leading SVs in the SA inner product are dominated by very small structures at the initialization time but systematically evolve toward large scales (comparable to those of the FVs) by the optimization time (Fig. 8a), where scale is measured by the mean wavenumber $\overline{K}$, defined by

$$\overline{K}^2 = \frac{\int |\boldsymbol{\nabla}\psi_1|^2 + |\boldsymbol{\nabla}\psi_2|^2 \, d\boldsymbol{x}}{\int \psi_1^2 + \psi_2^2 \, d\boldsymbol{x}}. \qquad (16)$$

In contrast, the leading WE and PV SVs have scales similar to those of the FVs at both initialization and optimization times with the WE SVs evolving toward
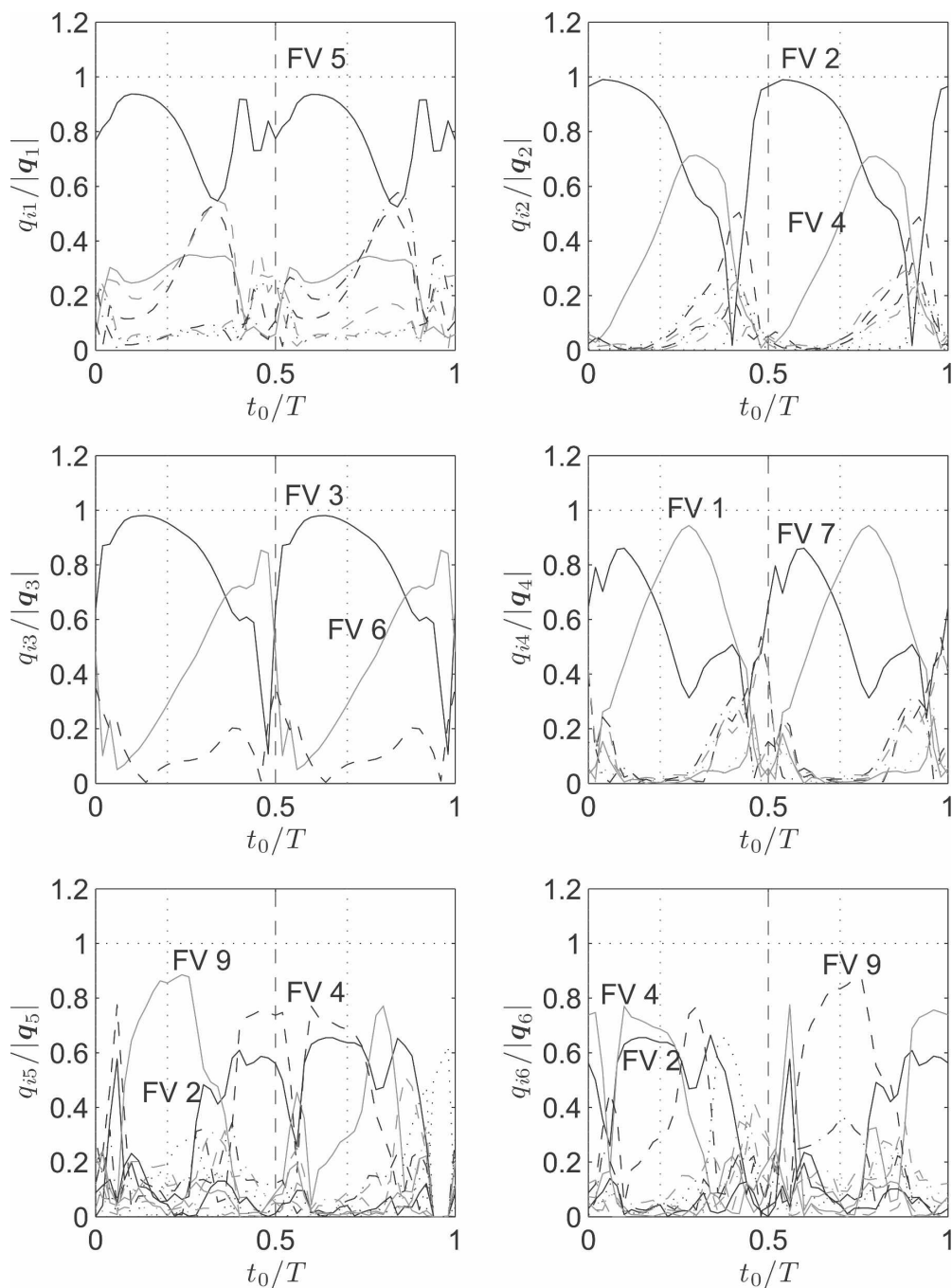
FIG. 7. As in Fig. 5 but for fixed optimization interval $\tau = T_w$. Only the largest few components have been labeled.

slightly larger scales (Fig. 8c) and the PV SVs evolving toward slightly smaller scales (Fig. 8e). While the similarity in scales between the initial WE and PV SVs and the FVs might suggest that these SVs are likely to project strongly onto the FVs, examination of their Floquet decompositions shows that this is not so: the leading initial SVs project not onto the leading FVs, but

onto the adjoint FVs. In all three cases, the most rapidly decaying SVs show evolution in the opposite sense as the leading SVs (Figs. 8b, 8d, and 8f).

The physical structures of the leading SVs are very similar to those found by other authors using global atmospheric models (e.g., Buizza et al. 1993; Buizza and Palmer 1995; Szunyogh et al. 1997; Vannitsem and Nic-
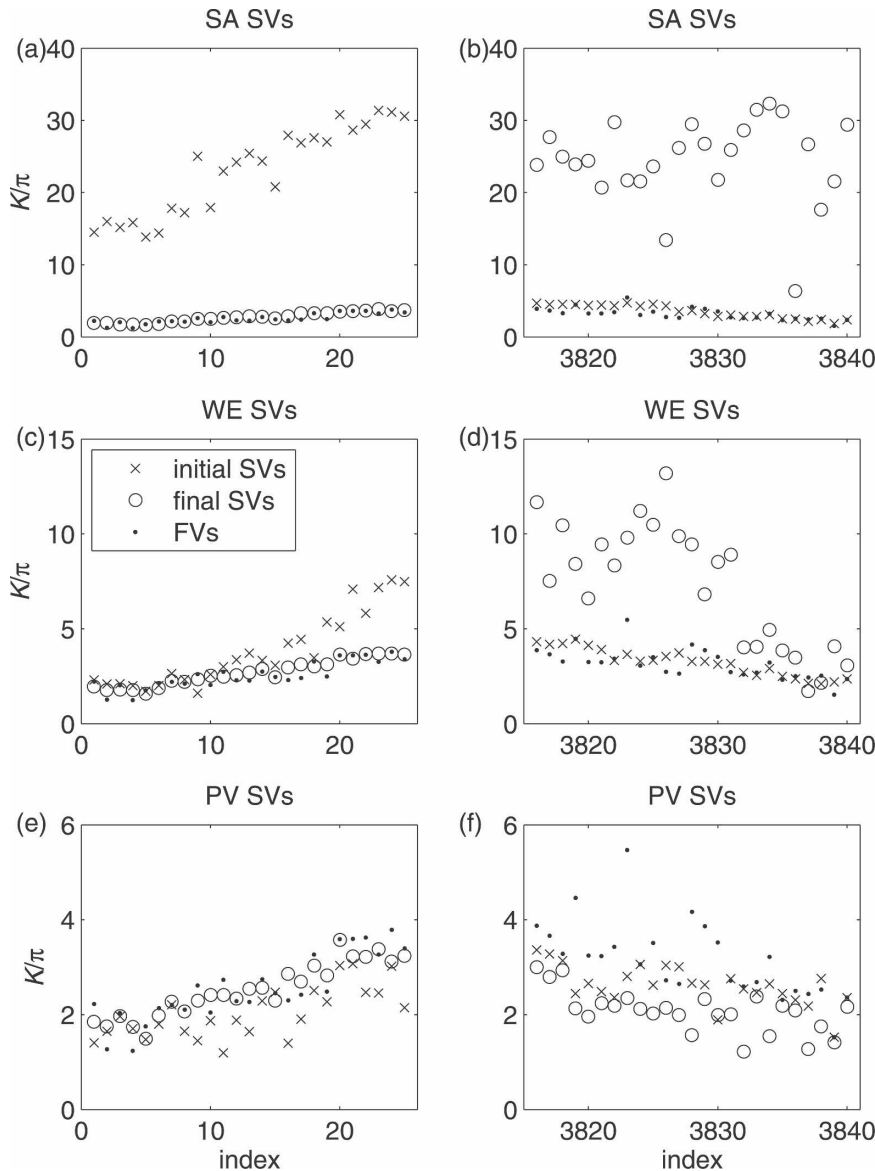
FIG. 8. Scales, as measured by mean wavenumber $\overline{K}$, of the leading and trailing SVs at the initialization (crosses) and optimization (circles) times for SVs calculated using the (a), (b) SA, (c), (d), WE, and (e), (f) PV inner products. The optimization interval $\tau = T$ and the results are averaged over all possible initialization times. The scales of the FVs (dots) are shown for reference.

olis 1997; Reynolds and Errico 1999) except that they are constrained by the channel geometry (corresponding roughly to a one-wavelength segment of one of the midlatitude jets) and by quasigeostrophy. The structures of the decaying SV are likewise very similar to those found by Reynolds and Palmer (1998) in their study of decaying SVs in a global quasigeostrophic model. Since the SVs have been so well described in previous studies and since the primary focus of this study in on the relationship of the SVs to the LVs and

the local attractor structure, we will omit a detailed discussion of the physical structures of the SVs.

4. Relationship to the local attractor structure

If a model used for ensemble forecasting is to be a faithful representation of the true dynamics of the atmosphere, the attractor of the model should resemble the attractor of the atmosphere. In that case, errors in the forecast should primarily be errors of placement

within the attractor. For lead times sufficiently short that disturbance dynamics are linear (2–3 days in the atmosphere), the initialization error should then lie in the unstable tangent linear space of the attractor. Thus, a common argument against using SVs in ensemble forecasting schemes is that the SV initial conditions point off (i.e., they are not geometrically tangent to) the attractor and that much of their growth is due to rapid rotation of the disturbances back onto the attractor (e.g., Kalnay 2003, section 6.3). The growing LVs (the aperiodic analog of FVs), on the other hand, determine a local unstable tangent linear space that represents the geometric tangent of the local attractor.

These statements are typically made in the context of low-dimensional systems and the behavior is generalized to much more complex systems evolving on high-dimensional attractors. In the present context—an intermediate complexity model evolving on a moderately high-dimensional attractor—these statements can be examined in a quantitative manner, both with regard to the unstable cycle and to the more complex chaotic attractor itself. The leading FVs define the local unstable tangent space to the basic cycle, and it is clear from the results of section 3 that the leading SVs do not project strongly into the subspace of the leading FVs but, instead, have strong projections onto the *adjoint* FVs. Thus, the leading SVs point "off" of the basic cycle and much of their initial growth comes from rapid rotation into the unstable subspace defined by the leading FVs.

It is of interest to determine if these results generalize to the attractor at large. We focus on trajectories within the attractor that are near the basic cycle in the following sense: Let the state vector formed by the basic cycle at the first cycle maximum be denoted by $\mathbf{P}_b$ and define a Poincaré section by the hyperplane passing through $\mathbf{P}_b$, which is orthogonal, in the sense of the SA inner product, to the tangent to the basic cycle $\partial_t \mathbf{P}_b$. Define $\Delta \mathbf{P}_j \equiv \mathbf{P}_j - \mathbf{P}_b$ as the difference between the Poincaré intersections and the basic cycle. The Poincaré intersections $\mathbf{P}_j$ with relative distance to $\mathbf{P}_b$,

$$d \equiv \frac{\|\Delta \mathbf{P}_j\|}{\|\mathbf{P}_b\|} \le 0.1, \qquad (17)$$

where $\|\cdot\|$ is the norm induced by the SA inner product, are considered to be "near" the basic cycle. Out of 120 000 Poincaré intersections, generated from a long integration on the attractor, 210 near approaches to the basic cycle satisfying (17) were found (Fig. 9). Since the attractor of the present system is a fairly high-dimensional object, any low period orbit represents only a part of the attractor, and this small number of returns is
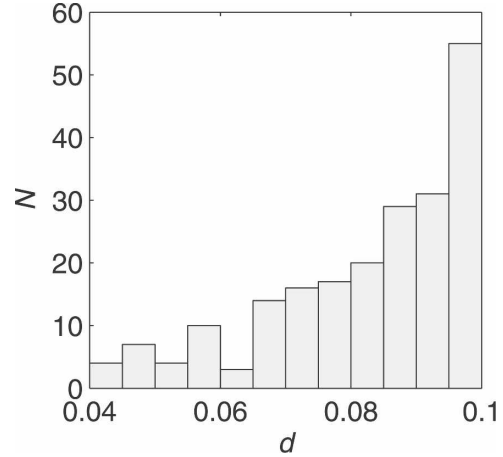

FIG. 9. Histogram of the relative d from the basic cycle $\mathbf{P}_b$ to the Poincaré intersections $\mathbf{P}_n$ based on 120 000 Poincaré intersections. The total number of intersections with $d \le 0.1$ is 210. There were no intersections with $d < 0.04$.

not a surprise. The 210 returns are nevertheless sufficient to furnish a useful description of the local structure of the attractor. Note that these and the following calculations were performed using a reduced resolution of 24×22 for computational expediency.

The extent to which the leading FVs describe the variability of nearby trajectories can be quantified by attempting to expand $\Delta \mathbf{P}_j$ in the leading n FVs:

$$\Delta \mathbf{P}_j = \sum_{i=1}^{n} \alpha_{ij} \phi_i + \boldsymbol{\rho}_j^{(n)}, \qquad (18)$$

where $\boldsymbol{\rho}_j^{(n)}$ is the residual after expanding $\Delta \mathbf{P}_j$ in the first n FVs. The determination of the expansion coefficients α_{ij} is complicated by the fact that the FVs are not orthogonal; however, they can be obtained as the unique minimizer of the functional

$$\mathcal{J}_j^{(n)} = \|\boldsymbol{\rho}_j^{(n)}\|^2 = \left\| \Delta \mathbf{P}_j - \sum_{i=1}^{n} \alpha_{ij} \hat{\phi}_i \right\|^2, \qquad (19)$$

where the $\hat{\phi}_i$ are the FVs projected into the Poincaré section. Note that, for orthonormal $\hat{\phi}$, minimization of $\mathcal{J}$ is equivalent to orthonormal expansion.

The relative magnitude of the residual gives the fraction of the variance of nearby Poincaré intersections left unexplained after expansion in the leading n FVs; thus,

$$f^{(n)} = 1 - \frac{\sqrt{\mathcal{J}_{j,\min}^{(n)}}}{\|\Delta \mathbf{P}_j\|} \qquad (20)$$

gives the fraction of the local variance explained by the leading n FVs. It is found that the leading 10 FVs ex-

plain approximately 90% of the local variance of $\Delta \mathbf{P}_j$, although there is significant point-to-point variability (Fig. 10). Note that very little improvement results from adding the fourth FV ϕ_4. This FV is the neutral mode proportional to $\partial_t \mathbf{P}_b$, which defines the normal to the Poincaré section. The $\Delta \mathbf{P}_j$ are thus orthogonal to ϕ_4 by construction.

The fraction of the local variability on the Poincaré section explained by the leading SVs may be similarly assessed by expanding $\Delta \mathbf{P}_j$ in terms of the leading SVs. The details of the calculation are unchanged. The initial conditions of the leading SVs do a poor job of describing the local variance, with little more than 25% of the variance captured by the WE and PV SVs and only about 2% captured by the SA SVs (Fig. 11, left panels). The initial WE and PV SVs explain significantly more of the local variance than the SA SVs because their spatial scales are much closer to those of the FVs than those of the SA SVs, as shown in section 3. In contrast, the SV final conditions capture as much of the variance as the FVs and show little variation between the three inner products (Fig. 11, right panels). This is consistent with the observation that the leading SVs project strongly on the leading FVs by the optimization time.

The above results demonstrate that, in addition to defining the local tangent space to the basic cycle, the leading FVs are also geometrically tangent to the local attractor structure; that is, they point onto the local attractor. On the other hand, the leading SV initial conditions point off of the local attractor, but rotate to become geometrically tangent to the local attractor by the optimization time.

5. Recovering Lyapunov vectors from singular vectors

The results of the previous section suggest that FVs and their generalizations, LVs, may be more useful than SVs for describing the behavior of trajectories that populate the phase space near a given control trajectory. In the present case, the LVs (here FVs) are available from a straightforward eigenvalue calculation and are used to calculate the SVs. For the more typical case of general time dependence, the FVs are not defined and the LVs are difficult to obtain. Standard techniques for calculating them require knowledge of $N + 1$, where N is the dimension of the system, asymptotically evolved and orthogonalized linear disturbances (usually SVs) to compute each LV, except for the most rapidly growing and decaying vectors (Legras and Vautard 1996; Trevisan and Pancotti 1998). For high-dimensional systems, computing $N + 1$ asymptotic SVs is typically beyond the capabilities of current comput-
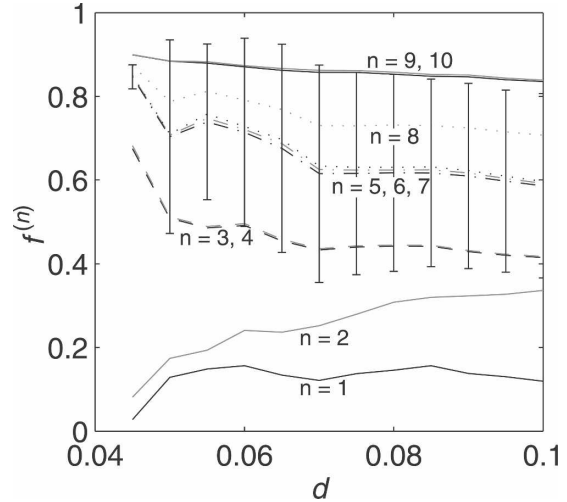

FIG. 10. Fraction of the local variance of $\mathbf{P}_n$ explained by the leading FVs $f^{(n)}$ ordered by the relative distance to the basic cycle d. Lines give bin averages of f and error bars (plotted on the $n = 5$ line) give bin standard deviations. The bin size is 0.005. The number of FVs n used to construct the leading subspace increases vertically, starting with $n = 1$ and ending with $n = 10$.

ing systems. Wolfe and Samelson (2007) have presented an efficient method for constructing the extremal n LVs using just $2n - 1$ SVs and demonstrated the effectiveness of this method using two low-dimensional numerical examples. If this method is effective in complex, high-dimensional systems, it would make a previously impossible calculation possible. The present model, with 3840 variables, provides an ideal system with which to begin testing this method. Furthermore, since the FVs are already known, they may be used to check the calculations. For a detailed discussion and justification of the method for recovering Floquet vectors from SVs, see Wolfe and Samelson (2007). A brief recapitulation is given here for completeness.

Fix a time t. Under fairly general conditions, SVs converge exponentially as $\tau \to \infty$ to constant linear combinations of the LVs (here, FVs). The convergence rate μ_n of the nth SV is estimated by

$$\mu_n = \begin{cases} |\lambda_2 - \lambda_1|, & n = 1 \\ \min\{|\lambda_{n+1} - \lambda_n|, |\lambda_n - \lambda_{n-1}|\}, & 1 < n < N \\ |\lambda_N - \lambda_{N-1}|, & n = N. \end{cases}$$

(21)

Note that, if the Floquet spectrum is degenerate, the SVs associated with multiple Floquet exponents will not exhibit exponential convergence to constant vectors and may not converge at all. Note, also, that complex conjugate Floquet exponents are considered degenerate according to this definition.
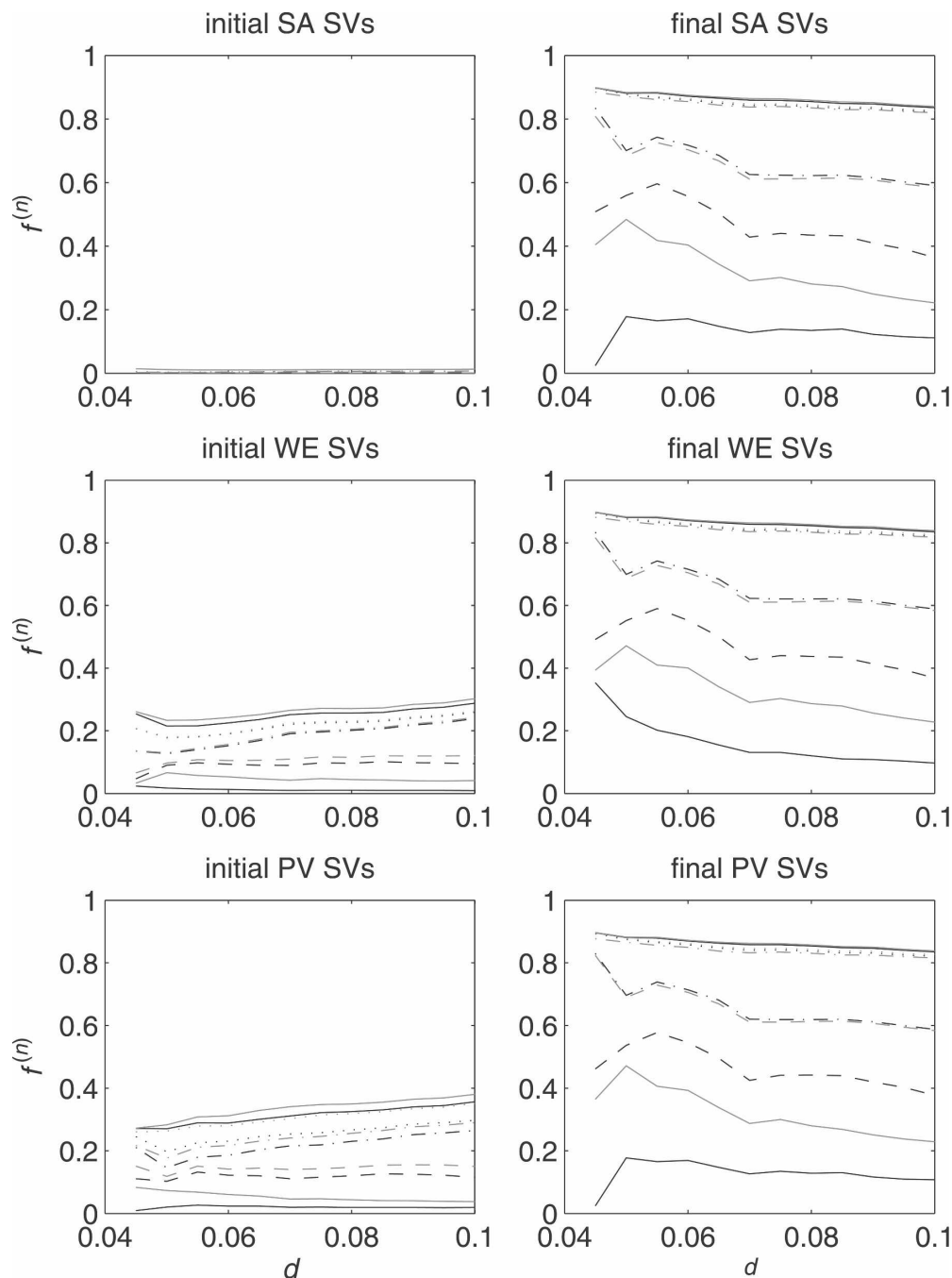
FIG. 11. Fraction f of the local variance of $\mathbf{P}_n$ explained by the leading SVs in the SA, WE, and PV norms, respectively, ordered by the relative distance to the basic cycle d. Lines give averages of f over bins of size 0.005. The number of SVs n used to construct the leading subspace increases vertically, starting with $n = 1$ and ending with $n = 10$.

In the present case, a large number ($\sim$3000) of FVs have complex Floquet exponents whose real parts cluster near the dissipation rate (WS), and, thus, the associated SVs are expected to converge very slowly (if at all) to their asymptotic forms. Fortunately, the Floquet exponents on the extreme upper and lower ends of the spectrum are real, distinct, and well separated, with two exceptions: First, FVs 4 and 5 are the two neutral modes and, thus, have $\lambda_4 = \lambda_5 = 0$. These modes are, however, orthogonal in the inner products used here, so
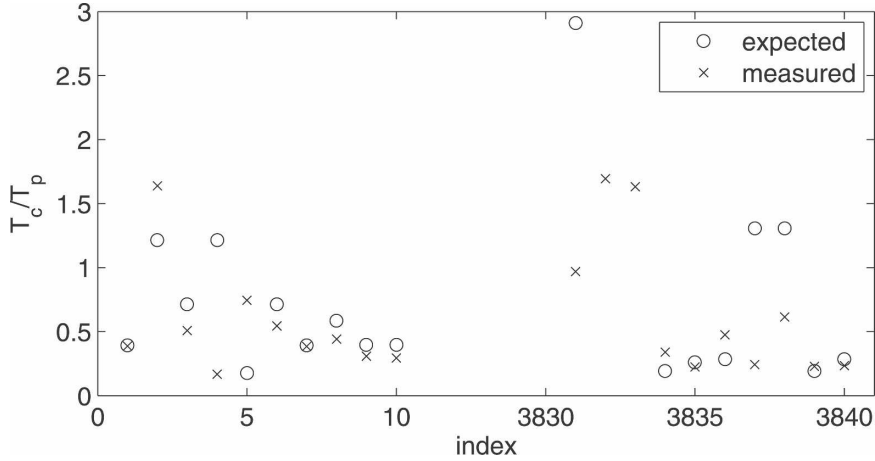
FIG. 12. Singular vector convergence *e*-folding time T_c relative to the period of the baroclinic wave–mean oscillation T. Circles give the expected convergence time based on the Floquet exponents; crosses give the average convergence time (based on an exponential fit). The asymptotic forms were only calculated for the first and last 10 SVs. For SVs 3832 and 3833, T_c is infinite.

the degeneracy of the Floquet exponents does not affect the convergence of the associated SVs. Thus, FV 5 (respectively, 4) was removed when calculating the convergence estimate (21) for FV 4 (respectively, 5). Second, FVs 3832 and 3833 form a complex conjugate pair, so $|\lambda_{3832}| = |\lambda_{3823}|$. These modes are thus degenerate and are not expected to converge in any finite time.

The first and last 10 SVs were calculated in the PV inner product for a fixed set of optimization intervals, with the longest interval $\tau = 3T$. The PV norm was chosen because it appeared to generate SVs with the fastest convergence rate. The order of magnitude of the convergence times is correctly estimated by Eq. (21), but do not agree with the estimated convergence time to the same degree as do the low-order examples of Wolfe and Samelson (2007) (Fig. 12). Some of the discrepancy may be due to the fact that—in contrast with the previous study—the present model is sufficiently computationally burdensome that the optimization interval was not systematically increased until convergence within a specified tolerance was observed. Thus, for some of the SVs, there may not be sufficient data to accurately estimate the observed convergence rate.

Let $\hat{\boldsymbol{\xi}}$ denote the initial conditions of SVs initialized at time t and optimized in the distant future and $\hat{\boldsymbol{\eta}}$ be the final conditions of SVs initialized in the distant past and optimized at time t. ["Distant past" and "distant future" should be taken to mean "long compared to the estimate Eq. (21)."] The method of Wolfe and Samelson (2007) allows the first n FVs to be recovered from $2n - 1$ asymptotic SVs by finding the nontrivial solution to

$$\mathbf{D}^{(n)}\mathbf{y}^{(n)} = 0, \qquad (22)$$

where

$$y_k^{(n)} = \langle \hat{\boldsymbol{\eta}}_k, \phi_n \rangle, \quad k = 1, 2, \ldots, n, \qquad (23)$$

$$D_{kj}^{(n)} = \sum_{i=1}^{n-1} \langle \hat{\boldsymbol{\eta}}_k, \hat{\boldsymbol{\xi}}_i \rangle \langle \hat{\boldsymbol{\xi}}_i, \hat{\boldsymbol{\eta}}_j \rangle, \quad k, j \le n. \qquad (24)$$

The recovered FV $\tilde{\phi}_n$ is then given by

$$\tilde{\phi}_n = \sum_{k=1}^{n} y_k^{(n)} \hat{\boldsymbol{\eta}}_k. \qquad (25)$$

The last n FVs may be obtained in a similar manner.

The FV $\tilde{\phi}$ recovered from the asymptotic SVs compare well with the FV ϕ calculated directly from the one-period propagator, with differences of order 1%–5% for the leading 10 FVs and trailing 7 FVs (Fig. 13); the slower convergence of FVs 3831–3834 is consistent with their longer convergence time scales (Fig. 12). This agreement demonstrates that the efficient method of Wolfe and Samelson (2007) can be used successfully to compute LVs from SVs in a model with several thousand degrees of freedom and multiple unstable modes. Curiously, while the leading 10 recovered FVs show a systematic improvement in accuracy as the optimization interval is increased, a number of the trailing FVs do not. This may be due to the fact the trailing FVs decay so rapidly (by more than 10^{-37} after three periods) that the numerical stability of the tangent linear integration and eigenvalue calculation are compromised for long optimization intervals. Since the leading
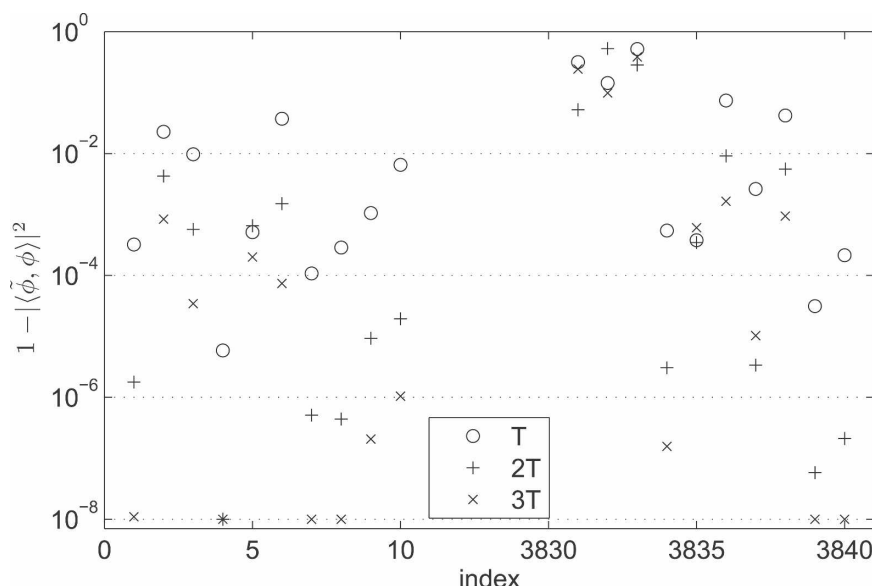
FIG. 13. One minus the pattern correlation between the recovered FVs $\tilde{\phi}$ and the true FVs ϕ for optimization intervals of T (circles), $2T$ (plus signs), and $3T$ (crosses), where T is the period of the basic wave–mean oscillation. A value of unity indicates orthogonality while a value of zero indicates collinearity. Pattern correlations for which $1 - |\langle\tilde{\phi}, \phi\rangle|^2 < 10^{-8}$ are plotted at 10^{-8} to show the upper values more clearly.

FVs/LVs are likely to be the most useful for predictability studies, the poor convergence properties of the rapidly decaying FVs/LVs are not of great concern.

6. Discussion

A significant advantage of the present calculations is that they allow the connection between normal mode disturbances (FVs) and optimal disturbances (SVs) to be explicitly displayed. The leading SVs are nonmodal disturbances: They have significant contributions from a large number of damped FVs and owe a significant portion of their initial growth to the rapid decay of the damped FVs. Further, as shown in section 4, the initial leading SVs point off the local attractor. It appears (Figs. 4 and 6) that the most rapidly damped SVs are modal, or nearly so, but this is an illusion. The largest components of the most rapidly damped SVs decay so quickly that, by the optimization time, the physical structure of these SVs will be dominated by less rapidly decaying FVs, no matter how small their initial projection onto the SVs.

The dynamical splitting observed in the present system is not as clear as that observed by Samelson (2001a,b) in a similar study of a weakly nonlinear model of the baroclinic instability. In that system, the dynamical splitting was so pronounced that the WD SVs projected strongly onto only the WD FVs. In that case, the primary transient growth mechanism for the leading SVs was interference between the inviscidly growing (leading) and inviscidly decaying (trailing) WD modes, which led Samelson to conjecture that inviscidly damped modes might be important for understanding the dynamics of transient error growth. In the present, less constrained system, we find that the leading SVs project primarily onto DA modes and weakly decaying WD modes. In fact, all of the SVs have strong projections onto FVs (either DA or WD modes) that decay at or faster than the dissipation rate, implying that the calculation of SVs from a leading subspace of normal modes is likely to produce highly suboptimal SVs.

The results of the present study are broadly consistent with those of Szunyogh et al. (1997) and Reynolds and Errico (1999), who also study the convergence of SVs to LVs. Both studies found that the leading SVs converge toward the leading LVs with a time scale of roughly one baroclinic life cycle. Detailed comparison of the results of the previous studies with the present contribution is complicated by the different definitions of the Lyapunov vectors used. For example, Reynolds and Errico (1999) used orthogonalized LVs estimated using 40-day SVs, while Szunyogh et al. (1997) considered only the convergence of the SVs to the first LV.

Accurate ensemble forecasting requires that the ensembles be initialized in such a way that their subse-

quent evolution is representative of the possible future states of the atmosphere. This initialization should also be economical so that the broadest possible set of future states is achieved by the smallest possible ensemble.

In the present case, the initial singular vectors point off the attractor and thus represent "unlikely" perturbations provided the forecast model is a reasonably good representation of the atmosphere. This may indicate that initial singular vectors are not a good choice for initial perturbations of ensemble members. On the other hand, the asymptotic stability of the basic cycle is determined by the leading LVs, so these modes are a natural choice for the ensemble initial conditions. The leading LVs have the advantage that they are few in number and that they are fluid instabilities that are related, in a straightforward manner, to the background flow (WS). This implies that the modes that are most interesting from the standpoint of geophysical fluid dynamical instability theory are also natural choices for ensemble initial conditions.

The results of section 3 indicate that, for optimization intervals greater than or equal to the baroclinic growth time scale, the leading final, or "evolved," singular vectors are approximately an orthogonalization of the leading LVs [this is also seen in studies of simpler models, e.g., Trevisan and Pancotti (1998); Wolfe and Samelson (2007)]. Thus, ensemble forecasting systems using the LVs and evolved singular vectors should behave roughly equivalently, all other things being equal. The choice between SVs and the LVs then becomes one of computational expediency. As discussed in section 5, current methods for estimating the leading LVs require knowledge of SVs with asymptotically long optimization intervals, making their computation significantly more expensive than the computation of short to midlength optimization interval SVs currently used in ensemble forecasting. However, since the LVs computed using the method outlined in section 5 are invariant under the tangent linear flow, it may be possible to reuse previously calculated LVs, reducing the effective burden of their computation. It is currently not clear whether this is sufficient to make LVs competitive, from an efficiency standpoint, with SVs. Experiments examining the feasibility of computing LVs in atmospheric GCMs are currently under way and may help resolve this question.

7. Summary

The SVs obtained in the present study characterize the transient growth of disturbances to a nonlinear wave-mean oscillation of a two-layer quasigeostrophic model. The model is simple enough to admit complete numerical solutions in terms of time-dependent normal modes (FVs), but, with several thousand degrees of freedom, complex enough to allow connections to be made to realistic operational forecast models. Much like the FVs of the same system (WS), the SVs divide into two dynamical classes. Singular vectors in the wave-dynamical class grow or decay at rates significantly different from the dissipation rate and exhibit large oscillations on the time scale of the baroclinic wave mean oscillation. The SV spectrum is completed by a large number of damped-advective modes that decay at rates near the dissipation rate.

For optimization times greater than the baroclinic wave growth time scale, the WD SVs asymptotically approach constant linear combinations of FVs. The most rapidly decaying SVs project strongly onto the most rapidly decaying FVs. In contrast, the leading SVs project strongly onto the leading adjoint FVs. The leading SVs are thus approximately optimal excitations of the leading FVs. Calculations where the initialization time was allowed to vary while the optimization interval was fixed to $\tau = T$ show that, while changes in the initialization time have a large impact on the singular values, they cause little change in the projection of the SVs onto the FVs. If the optimization interval is shortened to $\tau = T_w$, the FV decompositions of the most rapidly decaying SVs become complicated functions of initialization time, but the leading SVs remain relatively simple functions of the adjoint FVs.

Examination of Poincaré intersections near the basic cycle allows us to demonstrate, in a concrete and quantitative manner, that the leading FVs of the basic cycle are geometrically tangent to a local attractor. The leading initial SVs, by contrast, point off the attractor but rotate into the attractor by the optimization time. This demonstrates the value of LVs (here FVs) for describing the local structure of the attractor in a model of intermediate complexity and suggests they may be useful for even more complex models.

A method for recovering the leading LVs (here, FVs) from a relatively small number of SVs was demonstrated using the present calculations. While this system, used in the present study, is significantly more complex than those considered by Wolfe and Samelson (2007), the method was able to recover the leading LVs at a relative accuracy of 1% using SVs with $\tau = T$. Increasing the optimization time generally leads to significantly improved accuracy. This result suggests that the method may be robust enough for use in models with complexity comparable to operational forecast models.

REFERENCES

Buizza, R., and T. Palmer, 1995: The singular-vector structure of the atmospheric general circulation. *J. Atmos. Sci.,* **52,** 1434–1456.

——, J. Tribbia, R. Molteni, and T. Palmer, 1993: Computation of unstable structures for a numerical weather prediction model. *Tellus,* **45A,** 388–407.

——, and Coauthors, 2005: A comparison of the ECMWF, MSC, and NCEP global ensemble prediction systems. *Mon. Wea. Rev.,* **133,** 1076–1097.

Coddington, E. A., and N. Levinson, 1955: *Theory of Ordinary Differential Equations.* McGraw-Hill, 429 pp.

Cvitanović, P., R. Artuso, R. Mainieri, G. Tanner, and G. Vattay, 2005: *Chaos: Classical and Quantum.* Version 11. Neils Bohr Institute, Copenhagen, Denmark, digital media. [Available online at ChaosBook.org.]

Farrell, B. F., 1989: Optimal excitation of baroclinic waves. *J. Atmos. Sci.,* **46,** 1193–1206.

Kalnay, E., 2003: *Atmospheric Modeling, Data Assimilation, and Predictability.* Cambridge University Press, 341 pp.

Kazantsev, E., 1998: Unstable periodic orbits and attractor of the barotropic ocean model. *Nonlinear Processes Geophys.,* **5,** 193–208.

——, 2001: Sensitivity of the attractor of the barotropic ocean model to external influences: Approach by unstable periodic orbits. *Nonlinear Processes Geophys.,* **8,** 281–300.

Klein, P., and J. Pedlosky, 1986: A numerical study of baroclinic instability at large supercriticality. *J. Atmos. Sci.,* **43,** 1243–1262.

Lai, Y.-C., Y. Nagai, and C. Grebogi, 1997: Characterization of the natural measure by unstable periodic orbits in chaotic attractors. *Phys. Rev. Lett.,* **79,** 649–652.

Legras, B., and R. Vautard, 1996: A guide to Liapunov vectors. *Predictability,* T. Palmer, Ed., Vol. I, European Centre for Medium-Range Weather Forecasts, 143–156.

Lorenz, E. N., 1965: A study of the predictability of a 28-variable atmospheric model. *Tellus,* **17,** 321–333.

Miller, R. N., and L. L. Ehret, 2002: Ensemble generation for models of multimodal systems. *Mon. Wea. Rev.,* **130,** 2313–2334.

Oseledec, V., 1968: A multiplicative ergodic theorem: Lyapunov characteristic numbers for dynamical systems. *Trans. Moscow Math. Soc.,* **19,** 179–210.

Palmer, T. N., 1996: Predictability of the atmosphere and oceans: From days to decades. *Predictability,* T. Palmer, Ed., Vol. I,

European Centre for Medium-Range Weather Forecasts, 83–141.

Pedlosky, J., 1987: *Geophysical Fluid Dynamics.* 2nd ed. Springer, 710 pp.

Phillips, N. A., 1954: Energy transformations and meridional circulations associated with simple baroclinic waves in a two-level, quasi-geostrophic model. *Tellus,* **6,** 273–286.

Reynolds, C. A., and T. N. Palmer, 1998: Decaying singular vectors and their impact on analysis and forecast correction. *J. Atmos. Sci.,* **55,** 3005–3023.

——, and R. M. Errico, 1999: Convergence of singular vectors toward Lyapunov vectors. *Mon. Wea. Rev.,* **127,** 2309–2323.

Ruelle, D., 1979: Ergodic theory of differentiable dynamical systems. *IHES Publ. Math,* **50,** 27–58.

Samelson, R. M., 2001a: Lyapunov, Floquet, and singular vectors for baroclinic waves. *Nonlinear Processes Geophys.,* **8,** 439–448.

——, 2001b: Periodic orbits and disturbance growth for baroclinic waves. *J. Atmos. Sci.,* **58,** 436–450.

Samelson, R., and E. Tziperman, 2001: Instability of the chaotic ENSO: The growth-phase predictability barrier. *J. Atmos. Sci.,* **58,** 3613–3625.

Shimada, I., and T. Nagashima, 1979: A numerical approach to the ergodic problem of dissipative dynamical systems. *Prog. Theor. Phys.,* **61,** 1605–1616.

Stevens, M. R., and G. J. Hakim, 2005: Perturbation growth in baroclinic waves. *J. Atmos. Sci.,* **62,** 2847–2863.

Stoer, J., and R. Bulirsch, 2002: *Introduction to Numerical Analysis.* 3rd ed. Springer-Verlag, 744 pp.

Szunyogh, I., E. Kalnay, and Z. Toth, 1997: A comparison of Lyapunov and optimal vectors in a low-resolution GCM. *Tellus,* **49A,** 200–227.

Toth, Z., and E. Kalnay, 1993: Ensemble forecasting at NMC: The generation of perturbations. *Bull. Amer. Meteor. Soc.,* **74,** 2317–2330.

——, and ——, 1997: Ensemble forecasting at NCEP and the breeding method. *Mon. Wea. Rev.,* **125,** 3297–3319.

Trevisan, A., and F. Pancotti, 1998: Periodic orbits, Lyapunov vectors, and singular vectors in the Lorenz system. *J. Atmos. Sci.,* **55,** 390–398.

Vannitsem, S., and C. Nicolis, 1997: Lyapunov vectors and error growth patterns in a T21L3 quasigeostrophic model. *J. Atmos. Sci.,* **54,** 357–361.

Vastano, J. A., and R. D. Moser, 1991: Short-time Lyapunov exponent analysis and the transition to chaos in Taylor–Couette flow. *J. Fluid Mech.,* **233,** 83–118.

Wei, M., and J. S. Frederiksen, 2004: Error growth and dynamical vectors during Southern Hemisphere blocking. *Nonlinear Processes Geophys.,* **11,** 99–118.

Wolfe, C. L., and R. M. Samelson, 2006: Normal-mode analysis of a baroclinic wave-mean oscillation. *J. Atmos. Sci.,* **63,** 2795–2818.

——, and ——, 2007: An efficient method for recovering Lyapunov vectors from singular vectors. *Tellus,* **59A,** 355–366.

Zhang, Z., 1988: The linear study of zonally asymmetric barotropic flows. Ph.D. thesis, University of Reading, 178 pp.